Achieving and Sustaining Steady-State Advanced Tokamak Conditions on DIII–D

M.R. Wade,[1] M. Murakami,[1] D.P. Brennan,[2] T.A. Casper,[3] J.R. Ferron,[4] A.M. Garofalo,[5] C.M. Greenfield,[4] A.W. Hyatt,[4] R. Jayakumar,[3] J.E. Kinsey,[6] R.J. La Haye,[4] L.L. Lao,[4] E.A. Lazarus,[1] J. Lohr,[4] T.C. Luce,[4] C.C. Petty,[4] P.A. Politzer,[4] R. Prater,[4] E.J. Strait,[4] A.D. Turnbull,[4] J.G. Watkins,[7] and W.P. West[4]

[1]Oak Ridge National Laboratory, Oak Ridge, Tennessee, 37831 USA
email: wade@fusion.gat.com
[2]Oak Ridge Institute for Science Education, Oak Ridge, Tennessee 37831 USA
[3]Lawrence Livermore National Laboratory, Livermore, California 94551 USA
[4]General Atomics, P.O. Box 85608, San Diego, California, 92186-5608 USA
[5]Columbia University, New York
[6]Lehigh University, Bethlehem, Pennsylvania 18015 USA
[7]Sandia National Laboratories, P.O. Box 5800, Albuquerque, New Mexico 87185

Abstract. Recent experiments on the DIII–D tokamak have demonstrated the feasibility of sustaining advanced tokamak conditions that combine high fusion power density ($\beta > 4\%$), high bootstrap current fraction ($f_{BS} \sim 65\%$), and high non-inductive current fractions ($f_{NI} \sim 85\%$) for several energy confinement times. The duration of such conditions is limited only by resistive relaxation of the current density profile. Modeling studies indicate that the application of off-axis ECCD will be able to maintain a favorable current density profile for several seconds.

1. Introduction

Over the past several years, the Advanced Tokamak (AT) program on DIII–D has made significant progress towards demonstrating integrated AT plasma operation that simultaneously achieves high non-inductive current fractions and high fusion power density. This program's primary goal is to develop plasma scenarios that self consistently integrate and sustain the key ingredients of AT operation: high toroidal β_T at high q_{min}, good plasma confinement with $H_{89} \sim 2.5$, and high current drive efficiency. In recent years, significant progress has been made not only in understanding each of these elements separately but also in the interplay between the elements from an experimental, theoretical, and modeling perspective. Experiments have demonstrated the feasibility of sustaining advanced tokamak conditions that combine high fusion power density ($\beta_T = 2\mu_o \langle p \rangle / B_T^2 > 4\%$), high bootstrap current fraction ($f_{BS} \sim 65\%$), and high non-inductive current fractions ($f_{NI} \sim 85\%$) for several energy confinement times. The duration of such conditions is limited only by resistive relaxation of the current density profile. Simulations based on these plasmas indicate that the application of off-axis electron cyclotron current drive (ECCD) should be able to maintain a favorable current density profile for several seconds, provided integration of certain key elements (namely, density control at high β_T and efficient off-axis ECCD) can be achieved. In this paper, the status of AT research on DIII–D is summarized, focusing on those issues that we believe are essential for successful AT operation.

2. Maximizing β at $q_{min} >> 1$

The success of any AT approach that seeks to combine adequate fusion power density with a high bootstrap current fraction is predicated on operation at high β_T with $q_{min} >> 1$. This is due to the fact that the bootstrap current fraction scales as $f_{BS} \propto q^2 \beta_T$. Theoretical studies indicate that access to high β_T requires plasma shaping, broad pressure profiles, and the stabilization of external kink modes via use of, or mimicking, the effect of a perfectly conducting wall [1]. The effective beta limit may be lower than this ideal limit due to the destabilization of neoclassical tearing modes (NTMS) or other resistive MHD modes.

The temporal evolution of various waveforms for one of the best cases obtained to date on DIII–D is shown in Fig. 1. In this discharge, $\beta_N H_{89} > 10$ is maintained for several energy confinement times ($t_{dur} \sim 4 \tau_E$), with several excursions occurring in which $\beta_N \sim 4.1$ and H_{89}

~ 3.0 are achieved. At its maximum, β_T = 4.5%, which is approximately 50% above the nowall n=1 β limit, $\beta^{no\text{-}wall}$. Other figures of merit averaged over the high performance phase are: β = 4.3%, $\beta\tau_E$ = 0.7 %-s, β_p = 2.0, bootstrap current fraction f_{BS} = 65%, and non-inductive current fraction f_{NI} = 85%. Ultimately, the high performance phase is terminated by the destabilization of an m=2/n=1 NTM at 2.0 s as the current density profile evolves to an unstable state.

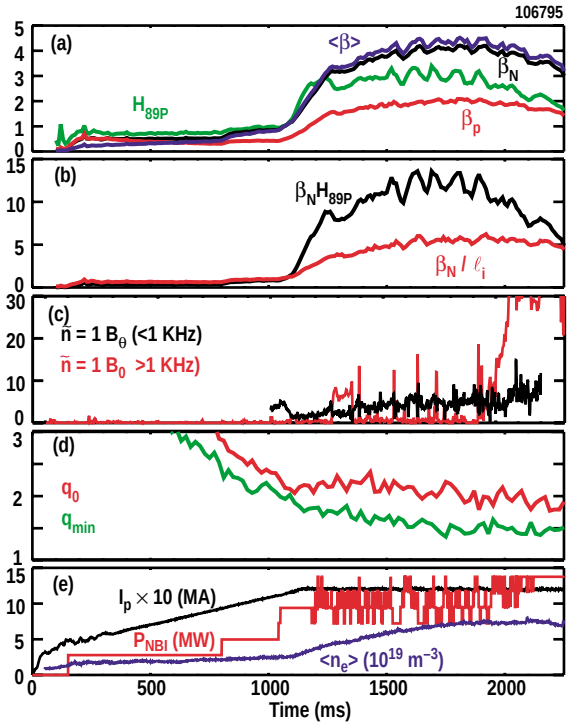

Fig. 1. Plasma parameters versus time for a discharge (106795) with $\beta_N H_{89}$ >10 for 4 τ_E (a) From top to bottom: <β>, β_N, H_{89}, and β_p, (b) From top to bottom: β_N H_{89} (upper trace), β_N/ℓ_i (lower trace); (c) n=1 Mirnov amplitude (G); (d) q_0 (upper trace), q_{min} (lower trace); (e) 10x plasma current (MA), neutral beam injected power (MW), line-averaged density (10^{19} m^{-3}).

Access to high β_T is made possible by simultaneously stabilizing resistive wall modes (RWMs) and avoiding NTMs. RWM stabilization takes on two forms: 1) stabilization by plasma rotation; and 2) direct feedback stabilization. Plasma rotation above a certain critical threshold is strongly stabilizing to RWMs while the effectiveness of direct feedback stabilization is dependent on the feedback scheme and its implementation [2–4]. Systematic studies have shown that similar levels of performance as that shown in Fig. 1 can be obtained by preprogramming the current in the segmented coils to the time-averaged currents obtained in the discharge shown in Fig. 1 (in which full feedback stabilization was used). This indicates that the primary stabilizing effect for RWMs in these plasmas is rotational stabilization. It is expected that the planned installation of internal feedback coils will significantly improve the effectiveness of active feedback stabilization.

With the RWMs stabilized, high β_T is maintained in Fig. 1 until the onset of an m=2/n=1 NTM at ~ 2 s. To avoid NTMs, careful optimization of the current and pressure profiles is essential. The case shown in Fig. 1 was arrived at through empirical optimization of the current density profile at the beginning of the high performance phase via variations in the heating profile, current ramp rate, and L-H transition timing during the current ramp. This optimization process determined that current profiles with q_0 slightly above 2 and q_{min} slightly below 2 at the beginning of the high performance phase were optimal for maximizing the attainable β_T and the duration over which such performance could be maintained.

The destabilization of the m=2/n=1 NTM in this class of discharges is quite different from that typically observed in q_0 ~ 1 plasmas. First, owing to the q_{min} > 1.5, there are no internal MHD events such as sawteeth or fishbones to produce seed islands of sufficient size to destabilize the tearing mode. Second, high β_p is generally sustained for several energy confinement times before the NTM onset. Third, the NTM onset typically occurs with β ~ $\beta^{no\text{-}wall}$ with q_{min} ~ 1.5. The first and second points suggests that the NTM trigger mechanism in this case is quite different from the typical q_0 ~ 1 case and that the leading order "neoclassical" terms in the modified Rutherford equation [5] (β_p, island width) are not playing a strong role in the destabilization process. If these terms were important, one would have expected the NTM onset to occur shortly after high β_p is established (rather than many hundreds of milliseconds later).

These observations are consistent with destabilization of the tearing mode by a rapid increase in Δ′ as an MHD stability boundary is approached [6]. Upon applying this theory to a

discharge very similar to the one shown in Fig. 1, good agreement is found between the timing of the proposed instability mechanism (a pole in Δ') and the destabilization of the NTM [see Fig. 2]. Further analysis indicates that near the occurrence of the pole in Δ' at 2.05 s, the sensitivity of Δ' to the magnetic equilibrium becomes extremely large as measured by the standard deviation in Δ' obtained by making random perturbations to the MSE diagnostic signals in the magnetic equilibrium reconstruction. The spike in sensitivity is indicative of the proximity of an MHD stability boundary since Δ' becomes extremely sensitive to the details of the magnetic equilibrium as an ideal MHD stability boundary is approached. Note that even after Δ' rapidly decreases after the onset of the mode, the tearing mode continues to grow, eventually saturating. This suggests that though the NTM is "seeded" by the rapid increase in Δ', the NTM grows and saturates in typical NTM fashion, governed by the neoclassical terms in modified Rutherford equation.

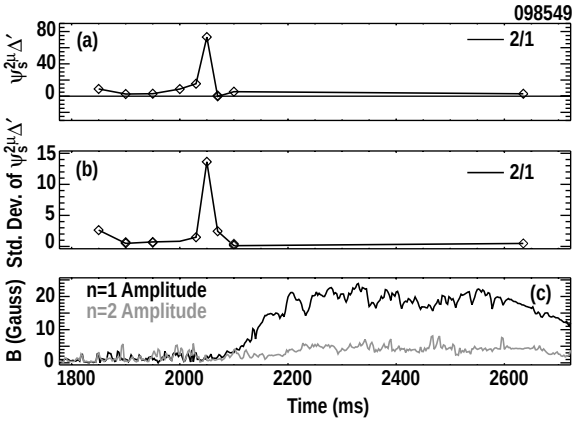

Fig. 2 Time history of (a) Δ' and (b) its standard deviation for a series of PEST-III [7,8] calculations based on magnetic equilibria constructed from the experimental data compared to the (c) observed MHD activity in the same discharge.

To obtain adequate density control for maximizing the current drive efficiency, active divertor exhaust is essential. In DIII–D, this is provided by the upper divertor, which is designed to allow particle exhaust in high triangularity, upper single-null plasma shapes. Unfortunately, the combination of a double-null (DN) shape and ion ∇B drift toward the lower divertor in the discharge shown in Fig. 1 makes it such that that the majority of the core particle efflux is directed to the lower divertor. Poor density control results and the density rises uncontrollably throughout the high performance phase [Fig. 1(e)]. Studies have shown that adequate particle control can be achieved by using a slightly, unbalanced upper single-null (USN) magnetic configuration and coupling to the upper divertor cryopumps. Initial use of the USN configuration in discharges similar to that shown in Fig. 1 have universally produced better density control but have also resulted in a reduction in attainable β_N compared to that obtained in balanced double-null shapes. Typically, an increase in the magnetic balance parameter dRsep (defined as the radial separation at the midplane of the field lines attached to the two nulls) from 0 to 1 cm without making any other changes in the plasma shaping algorithm results in a 10% reduction in the achievable β_N. By increasing the plasma shaping by pulling the lower divertor X–point radially inward and vertically down, the q_{95} of the DN case can be recovered with dRsep = 1 cm. Using this magnetic configuration, experiments have demonstrated the ability to simultaneously obtain good density control with β_N approximately the same as the best DN cases. However, the duration of the high performance phase is generally reduced by earlier onset of a m=2/n=1 NTM.

3. Maximizing the Non-Inductive Current Density

Because of the importance of the current profile in AT plasmas, the ability to dynamically modify and sustain the current profile at high β_T is a prerequisite for successful AT operation. The primary source of external current drive on DIII–D is electron cyclotron current drive (ECCD). In the 2002 experimental campaign, five gyrotrons each capable of delivering over 750 kW of power were connected to steerable launchers on DIII–D. Through poloidal steering of these launchers, the radial location at which the EC power is deposited can be controlled. AT scenarios seek to take advantage of this flexibility by using ECCD to provide off-axis current drive, increasing the local current density to produce very low or negative magnetic shear in the plasma center. Off-axis current drive is known to be less efficient than on-axis current drive due to the T_e/n_eR scaling of the current drive efficiency and to increased electron trapping. Because of this, it is imperative that the physics of ECCD be well understood so that the maximum ECCD current drive can be obtained for a given EC

power. Extensive studies of the various physics phenomena governing ECCD current drive have been conducted on DIII–D and are summarized in Ref. [12]. Of particular interest to AT scenario development is the observed increase of the normalized current drive efficiency as β_e is increased. These studies indicate that the normalized current drive efficiency increases as approximately $\beta_e^{1/2}$, arising from Doppler shifting of the resonance location in velocity space so that the EC power is absorbed by electrons that are further away from the trapped electron boundary than would be the case with $\beta_e = 0$. Including this effect, the overall current drive efficiency can then be written $\eta_{ECCD} \propto (T_e/n_eR)\beta_e^{1/2}$

In order to maximize the total non-inductive current drive, one would like to simultaneously maximize η_{ECCD} and the self-generated bootstrap current. For similar plasma density and temperature profiles, the bootstrap current is maximized by maximizing β_p. Although β_p values consistent with the DIII–D AT target have been obtained, the best current drive efficiency is still a factor of three smaller than desired (Fig. 3). Thus, even in cases with good density control, an unacceptable value for η_{ECCD} is obtained. These low values of η_{ECCD} at low density are believed to be due to a reduction in β_e as the density is lowered. Evidence for this is shown graphically in Fig. 4 where a measure of the overall current drive efficiency parameter $(T_e/n_e)\beta_e^{1/2}$ is plotted versus plasma density, each measured at $\rho = 0.5$. An inverse dependence of $(T_e/n_e)\beta_e^{1/2}$ with density is observed, which lies between a "best-case" scenario (with β_e constant with density) and a "worst-case" scenario (with T_e constant with density). The likely reason for this degradation is the predominance of NBI heating in the AT studies to date.

Despite these challenges in simultaneously obtaining high β_p and η_{ECCD}, experiments have demonstrated the ability to control the current density profile for periods as long as 1 s. Figure 5 shows one of the best cases obtained so far along this line. For this discharge, a slightly unbalanced upper single-null configuration with dRsep = 0.5 cm was used. The discharge was arrived at differently from the one in Fig. 1, with an H–mode induced early in the current ramp. Nevertheless, the *q* profile at the beginning of the high performance phase (2.8 s) is nearly identical to that as the discharge in Fig. 1. Subsequently, $\beta_N = 3.1$ is maintained by feedback control of the NBI power. Approximately 2.5 MW of co-directed ECCD resonant on the inboard midplane at $\rho = 0.4$ is applied starting at 3.0 s. Between 3.0 and 4.0 s, the current density profile is observed to be nearly constant with $q_0 \sim 2.1$ and $q_{min} \sim 1.7$. Analysis of the poloidal flux evolution indicates that even though the ECCD does not modify the current density profile, it does produce a drop in the loop voltage inside the resonance location. The total non-inductive current drive in this case approaches 95% with 65% of the plasma current provided by bootstrap current, 20% by neutral beam current

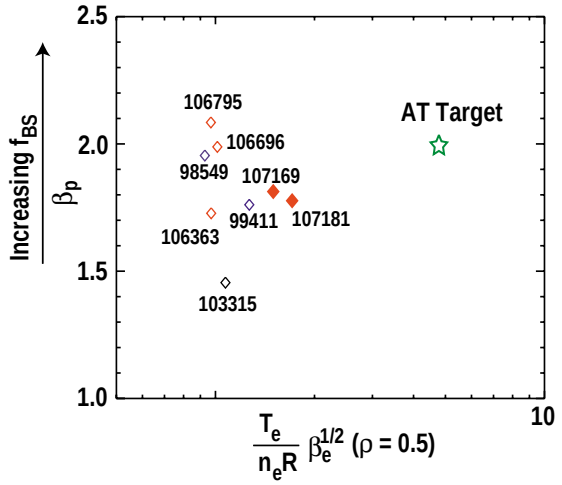

Fig.3 β_p versus $(n_e/T_e)\beta_e^{1/2}$ at $\rho = 0.5$. All discharges have $\beta_N > 4\,\ell_i$. Star denotes AT target design point.

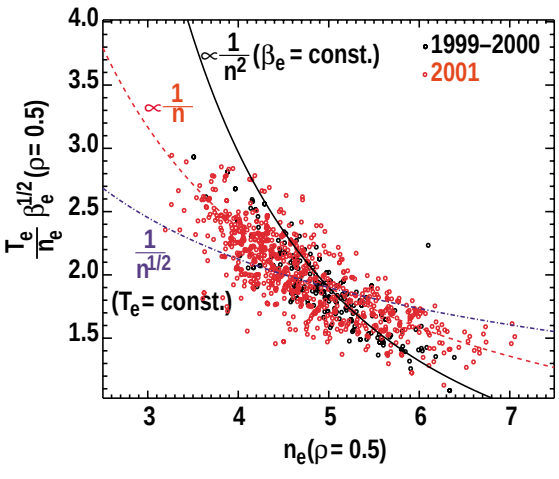

Fig. 4. Data points represent measured current drive efficiency parameter $(n_e/T_e)\beta_e^{1/2}$ at $\rho = 0.5$ versus plasma density. Possible dependencies of the current drive efficiency are denoted by the curves.

drive, and 10% by ECCD. The remaining Ohmic current is peaked off-axis. Hence, with careful optimization of the ECCD deposition location, replacement of this current should also be possible.

4. Modeling

In conjunction with the extensive AT experimental effort on DIII–D, considerable effort has been made in applying the experimental knowledge to developing improved AT scenarios through modeling and simulations. These simulations, utilizing a suite of transport codes (ONETWO/CalTrans/TRANSP) and an ECCD ray-tracing code (TORAY), strive to be as self-consistent as possible, using plasma profiles and transport coefficients consistent with those obtained experimentally. The primary goal of this effort has been to determine under what conditions a favorable current density profile can be maintained using the available EC power on DIII–D. Time-dependent transport simulations indicate that a favorable current profile (similar as that obtained before the onset of the NTM in Fig. 1) can be maintained for ~ 10 s (or twice the current redistribution time) using 3.5 MW of ECCD distributed broadly off-axis (Δ_{FWHM}=0.27 centered at ρ_{EC}=0.38). To allow for the effect of the additional heating provided by ECCD, the transport coefficients are degraded from those obtained in the experiment in a manner such that the transport coefficients scale as would be expected by the ITER H98-ELYy2 scaling [12] expression ($\chi \sim P^{+0.69}$). Studies of the sensitivity of the obtained results to the prescribed transport coefficients have shown that the favorable q profile can be maintained even with χ_e and χ_i increased by a factor of 2 for $\rho \leq 0.8$ over the base case.

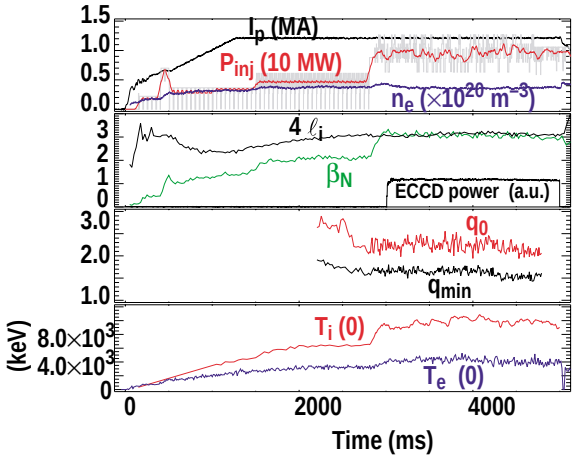

Fig. 5. Plasma parameters versus time for a discharge in which ECCD was used to sustain the current density profile: (a) plasma current, actual and smoothed neutral beam injected power, and line-averaged density; (b) β_N, 4 ℓ_i, and ECCD power; (c) q_0 and q_{min}; and (d) central ion and electron temperatures.

5. Summary

Experiments on DIII–D have demonstrated the feasibility of achieving Advanced Tokamak conditions that sustain high fusion power density (β_T > 4%) and a high bootstrap current fraction (f_{BS} ~ 65%) for several energy confinement times. The termination of these conditions is due to the resistive evolution of the current profile, leading to the onset of NTMs as q_{min} approaches 1.5. Having demonstrated the feasibility of the major elements required for efficient off-axis ECCD (namely, sustained high β_T, density control, and efficient ECCD) separately, the DIII–D program is now focussed on the self-consistent integration of these elements into a steady-state, high fusion gain plasma solution.

Work supported by U.S. Department of Energy under Contracts DE-AC05-00OR22725, W-7405-ENG-48, DE-AC03-99ER54463, DE-AC04-94AL85000, and Grants DE-FG02-89ER53297, and DE-FG02-92ER54141.

[1] T.S. Taylor, et al., Plasma Phys. Controlled Fusion **39** B47 (1997).
[2] A.M. Garofalo, et al, Phys. Plasmas **9**, 1997 (2002).
[3] E.J. Strait, et al., this conference.
[4] M. Okabayashi, et al., Phys. Plasmas **8**, 2071 (2001).
[5] H.R. Wilson, J.W. Connor, R.J. Hastie, C.C. Hegna, Phys. Plasmas **3**, 248 (1996).
[6] D.P. Brennan, Phys. Plasmas **9**, 2998 (2002).
[7] R.L. Dewar and A. Pletzer, J. Plasma Phys. **43**, 291 (1990).
[8] A. Pletzer and R.L. Dewar, J. Plasma Phys. **45**, 427 (1991).
[9] M.R. Wade, et al., Phys. Plasmas **8**, 2208 (2001).
[10] T.C. Luce, et al., Nucl. Fusion **41**, 1585 (2001).
[11] A.D. Turnbull, et al., Nucl. Fusion **38**, 1467 (1998).
[12] C.C. Petty, et al., this conference.
[13] ITER Physics Basis, Nucl. Fusion **39**, 2175 (1999).